Article

Description of the Ground State Wave Functions of Ni Dithiolenes Using Sulfur K-edge X-ray Absorption Spectroscopy

Robert K. Szilagyi, Booyong S. Lim, Thorsten Glaser, Richard H. Holm, Britt Hedman, Keith O. Hodgson, and Edward I. Solomon

J. Am. Chem. Soc., **2003**, 125 (30), 9158-9169• DOI: 10.1021/ja029806k • Publication Date (Web): 04 July 2003

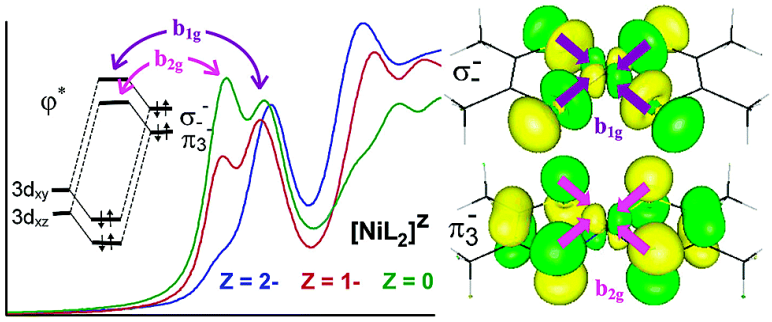

More About This Article

Additional resources and features associated with this article are available within the HTML version:

- Supporting Information
- Links to the 16 articles that cite this article, as of the time of this article download
- Access to high resolution figures
- Links to articles and content related to this article
- Copyright permission to reproduce figures and/or text from this article

View the Full Text HTML

J|A|C|S
ARTICLES
Published on Web 07/04/2003

Description of the Ground State Wave Functions of Ni Dithiolenes Using Sulfur K-edge X-ray Absorption Spectroscopy

Robert K. Szilagyi,[†] Booyong S. Lim,[‡] Thorsten Glaser,[†,||] Richard H. Holm,*[,‡] Britt Hedman,*[,§] Keith O. Hodgson,*[,†,§] and Edward I. Solomon*[,†]

Contribution from the Department of Chemistry, Stanford University, Stanford, California 94305, Department of Chemistry and Chemical Biology, Harvard University, Cambridge, Massachusetts 02138, Stanford Synchrotron Radiation Laboratory, SLAC, Stanford University, Stanford, California 94309

Received December 19, 2002; E-mail: holm@chemistry.harvard.edu; Hedman@SLAC.Stanford.Edu; Hodgson@SLAC.Stanford.EDU; Edward.Solomon@Stanford.EDU

Abstract: The pterin-dithiolene cofactor is an essential component of the catalytic sites of all molybdoenzymes except nitrogenase. Understanding its bonding to transition metals allows for development of electronic structure/function correlations in catalysis. The electronic structure description for a series of bis(dithiolene) complexes ($[NiL_2]^Z$, L = 1,2-$Me_2C_2S_2$; $Z = 2-, 1-, 0$) using sulfur XAS provides the basis for extension to the biologically relevant metal-containing dithiolenes. The transition dipole integral has been developed for the dithiolene sulfur through correlation of XAS pre-edge energy positions of sulfide-, thiolate-, and enedithiolate-S. The ground state wave functions of all three NiL_2 complexes have more than 50% S character experimentally demonstrating the noninnocent behavior of the dithiolene ligand. The S K-edge experimental results are correlated with spin-unrestricted, broken-symmetry density functional calculations. These show only limited spin polarization in the neutral complex and delocalized, ligand based ground states for the mono- and dianionic complexes. These XAS and DFT results are correlated with other spectroscopic features and provide insight into reactivity.

Introduction

Transition metal bound thiolates play essential roles in bioinorganic electron transfer and catalytic processes.[1] Understanding the bonding between sulfur and metal atoms is important in gaining insight into structure/function relationships. Structurally well-characterized, stable thiolate complexes are ideal systems to study as biomimetic active site models. The Ni−S bond is well understood in thiolate complexes;[2] however, the ground state descriptions of the Ni bis(dithiolene)[3] complexes $[Ni(S_2C_2R_2)_2]^{2-,1-,0}$, where R = H, CH_3, CF_3, CN, and so forth, have been the subject of considerable discussion.[4−10] The bonding in the monoanionic complex could be quantitated experimentally as it is paramagnetic with $S = {}^1/_2$ and, therefore, ideal for EPR[8,11] and ENDOR/ESEEM[12] spectroscopies. In general, the monoanionic complex is characterized by a highly covalent bonding with the spin delocalized over the ligands. The spin on the $[NiS_4]$ core was quantitated to be 85% with a metal contribution of approximately 25%.[12] This was one of the first direct indications of the noninnocent nature of the dithiolene ligand. Other than electronic absorption spectra[9,10] and a few computational studies[13−15] (mainly focusing on geometric structure), less is known about the bonding in the dianionic and the neutral Ni dithiolene complexes. The dianionic complex has been considered to be a normal Ni^{II} complex with two dianionic ene-1,2-dithiolate ligands.[16] For the neutral complex, two plausible electronic structure descriptions have been discussed in the literature,[17,18] both assuming a Ni^{II} formal

[†] Department of Chemistry, Stanford University.
[‡] Department of Chemistry and Chemical Biology, Harvard University.
[§] Stanford Synchrotron Radiation Laboratory, SLAC, Stanford University.
[||] Present address: Institute fuer Anorganische und Analytische Chemie, Westfalische Wilhelms-Universitaet Muenster, Germany.

(1) Holm, R. H.; Kennepohl, P.; Solomon, E. I. *Chem. Rev.* **1996**, *96*, 2239−2314.
(2) Williams, K. R.; Hedman, B.; Hodgson, K. O.; Solomon, E. I. *Inorg. Chim. Acta* **1997**, *263*, 315−321.
(3) Throughout the text, the free $[S_2C_2R_2]^{2-}$ ligand and its metal-bound form are referred as the enedithiolate ligand and the dithiolene complex, respectively.
(4) McCleverty, J. A. *Prog. Inorg. Chem.* **1968**, *10*, 49−221.
(5) Schrauzer, G. N. *Acc. Chem. Res.* **1969**, *2*, 72−80.
(6) Eisenberg, R. *Prog. Inorg. Chem.* **1970**, *12*, 295−369.
(7) Hoyer, E.; Dietzsch, W.; Kirmse, R.; Hoyer, E. *Coord. Chem. Rev.* **1992**, *117*, 99−348.
(8) Maki, A. H.; Edelstein, N.; Davison, A.; Holm, R. H. *J. Am. Chem. Soc.* **1964**, *86*, 4580−4587.
(9) Shupack, S. I.; Billig, E.; Clark, R. J. H.; Williams, R.; Gray, H. B. *J. Am. Chem. Soc.* **1964**, *86*, 4594−4602.
(10) Schrauzer, G. N.; Mayweg, V. P. *J. Am. Chem. Soc.* **1965**, *87*, 3585−3592.
(11) Schmitt, R. D.; Maki, A. H. *J. Am. Chem. Soc.* **1968**, *90*, 2288−2292.
(12) Huyett, J. E.; Choudhury, S. B.; Eichhorn, D. M.; Bryngelson, P. A.; Maroney, M. J.; Hoffman, B. M. *Inorg. Chem.* **1998**, *37*, 1361−1367.
(13) Kraffert, C.; Walther, D.; Peters, K.; Lindqvist, O.; Langer, V.; Sieler, J.; Reinhold, J.; Hoyer, E. *Z. Anorg. Allg. Chem.* **1990**, *588*, 167−180.
(14) Arca, M.; Demartin, F.; Devillanova, F. A.; Garau, A.; Isai, F.; Lelj, F.; Lippols, V.; Pedraglio, S.; Verani, G. *J. Chem. Soc., Dalton Trans.* **1998**, 3731−3736.
(15) Lauterback, C.; Fabian, J. *Eur. J. Inorg. Chem.* **1999**, 1995−2004.
(16) Holm, R. H.; O'Connor, M. J. *Prog. Inorg. Chem.* **1971**, *14*, 241−401.
(17) Stiefel, E. I.; Waters, J. H.; Billig, E.; Gray, H. B. *J. Am. Chem. Soc.* **1965**, *87*, 3016−3017.
(18) Balch, A. L.; Holm, R. H. *J. Am. Chem. Soc.* **1966**, *88*, 5201−5209.

10.1021/ja029806k CCC: $25.00

Scheme 1

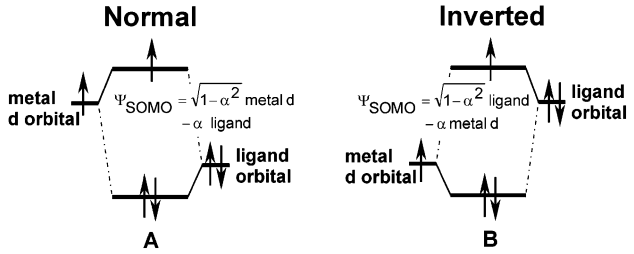

oxidation state for the metal. One of the bonding descriptions assumes a diradical, localized ground state with the unpaired electrons located on the ligands (mainly on the αC atoms attached to the S atoms), while the other describes the electronic structure as a delocalized resonance pair between enedithiolate and dithioketone ligand forms.

A recent study[19] has provided the first complete series of nonbenzenoid Ni bis(dithiolene) complexes over three oxidation states with the same dithiolene ligand, $[Ni(S_2C_2Me_2)_2]^Z$, $Z = 2-$, $1-$, and 0, which is the subject of this investigation. In addition to experimental structural characterization, the electronic structures of these complexes have been studied by gradient-corrected density functional calculations (BP86/BSIV), which gave good agreement in bond lengths and angles within 0.03 Å and 0.6°, respectively. The experimental *g*-values for the paramagnetic complex ($Z = 1-$) were reproduced within 0.031. The singly occupied orbital was identified as the antibonding combination of mainly S $3p_z$ and Ni $3d_{xz}$ orbitals. On the basis of changes in electronic structure, geometry, and stretching frequencies, it was concluded that a Ni^{II} formal oxidation state is appropriate for the dianion complex and the diradical state is not accessible at room temperature for the neutral Ni dithiolene complex.

Bachler et al.[20] have studied the electronic structure of the neutral, ortho-semiquinonato type Ni complexes with O-, N-, and S-ligands employing hybrid density functional (B3P86 and B3LYP/SDD) and multireference ab initio (CASSCF(2e,8o)/SDD) calculations. The broken symmetry B3LYP wave functions of the neutral complexes show increasing diradical character upon going from S to N and to O in a qualitative agreement with the CASSCF results. At these levels of theory, the diradical character of the neutral Ni dithiolene complex is practically zero.[20] However, electronic structure descriptions by hybrid DFT calculations can be strongly dependent on the amount of Hartree−Fock exchange (HFX),[21] which needs to be calibrated spectroscopically.

Ligand K-edge X-ray absorption spectroscopy (XAS)[22,23] is a direct method to address bonding and covalency in metal complexes. In a normal bonding scheme (Scheme 1A), where the metal orbitals are destabilized relative to the ligand orbitals, increase in the ligand character (α^2) of the ground state wave function corresponds to more covalent bonding. Using tunable synchrotron radiation in an energy range around 2472 eV, the sulfur core 1s electron can be excited into the unoccupied S 4p orbitals and to the continuum giving rise to an electric-dipole-allowed edge feature. In addition, transitions into the unoccupied or half-occupied orbitals of the d-manifold are generally at lower energy than the edge jump and can gain intensity proportional to their S 3p character. The intensity of these pre-edge features can be quantitated based on expression (1)

$$D_0(\text{S 1s} \rightarrow \varphi^*) = \text{constant } |\langle \text{S 1s } |\mathbf{r}| \, \varphi^* \rangle|^2 = \alpha^2 \, I(\text{S 1s} \rightarrow \text{3p}) \quad (1)$$

where D_0 is the normalized intensity taking into account the number of absorbers and degeneracy of the unoccupied orbital holes, **r** is the transition dipole operator, and α^2 is the amount of ligand character (i.e., covalency) of the unoccupied orbital, $\varphi^* = (1 - \alpha^2)^{1/2}|\text{metal 3d}\rangle - \alpha \, |\text{S 3p}\rangle$ (Scheme 1A).

To quantitate the S covalency in an unoccupied orbital, the transition dipole integral, I(S 1s→3p) needs to be determined for the enedithiolate-S and for the covalently bound dithiolene ligand. These experimental covalencies for the three Ni dithiolenes can also be correlated with density functional calculations. As shown for Cu-containing systems,[21,24] the density functional that best correlates to experiment depends on the metal oxidation and spin state. The spectroscopically adjusted DFT calculations for the Ni dithiolenes can give further insight into geometric structure, spin distribution, spin polarization, and reactivity. With respect to the latter, Wang and Stiefel have recently introduced a novel approach for olefin separation and purification using Ni dithiolene complexes.[25]

Experimental Section

A. Sample Preparation. The complexes $[Ni(S_2C_2Me_2)_2]^Z$, $Z = 2-$, $1-$, 0 and the disodium salt of the simplest enedithiolate ($Na_2S_2C_2H_2$) were prepared as described previously.[19,26,27] A salt of the free ligand $[S_2C_2Me_2]^{2-}$ has not yet been isolated. The sodium salts of the sulfide (Na_2S) and ethylthiolate ($NaSC_2H_5$) ligands were purchased from Sigma−Aldrich Co.

B. X-ray Absorption Measurement and Data Analysis. The S K-edge data were measured at the Stanford Synchrotron Radiation Laboratory under ring conditions of 3 GeV and 60−100 mA. The measurements utilized the 54-pole wiggler beam line 6−2 operating in high field mode of 10 kG with a Ni-coated harmonic rejection mirror and a fully tuned Si(111) double crystal monochromator. Details of the beam line optimization for S K-edge studies were published elsewhere.[28] The solid samples were ground in a drybox at less than 1 ppm O_2 level and dispersed as thinly as possible on a Mylar tape to minimize the possibility of fluorescence saturation effects. A 6 μm thick, S-free polypropylene window was used to prevent sample exposure to air upon mounting into the sample chamber. The spectra were measured as fluorescence excitation spectra utilizing an ionization chamber as a fluorescence detector.[29,30] The photon energy was calibrated to the maximum of the first pre-edge feature of $Na_2S_2O_3 \cdot 5H_2O$ at 2472.02 eV. In the case of photoreduction (spectrum changes with time during measurement), as observed for the $[Ni(S_2C_2Me_2)_2]^{2-}$ complex, an

(19) Lim, B. S.; Fomitchev, V.; Holm, R. H. *Inorg. Chem.* **2001**, *40*, 4357−4262.
(20) Bachler, V.; Olbrich, G.; Neese, F.; Wieghardt, K. *Inorg. Chem.* **2002**, *41*, 4179−4193.
(21) Szilagyi, R. K.; Metz, M.; Solomon, E. I. *J. Chem. Phys. A* **2002**, *106*, 2994−3007.
(22) Hedman, B.; Hodgson, K. O.; Solomon, E. I. *J. Am. Chem. Soc.* **1990**, *112*, 1643−1645.
(23) Glaser, T.; Hedman, B.; Hodgson, K. O.; Solomon, E. I. *Acc. Chem. Res.* **2000**, *33*, 859−868.
(24) Szilagyi, R. K.; Solomon, E. I. *Curr. Opin. Chem. Biol.* **2002**, *6*, 250−258.
(25) Wang, K.; Stiefel, E. I. *Science* **2001**, *291*, 106−109.
(26) Schroth, W.; Peschel, J. *Chimia* **1964**, *18*, 171−123.
(27) Schrauzer, G. N.; Mayweg, V. P. *J. Am. Chem. Soc.* **1965**, *87*, 1483−1489.
(28) Hedman, B.; Frank, P.; Gheller, S. F.; Roe, A. L.; Newton, W. E.; Hodgson, K. O. *J. Am. Chem. Soc.* **1988**, *110*, 3798−3805.
(29) Stern, E. A.; Heald, S. M. *Rev. Sci. Instrum.* **1979**, *50*, 1579−1582.
(30) Lytle, F. W.; Greegor, R. B.; Sandstrom, D. R.; Marques, E. C.; Wong, J.; Spiro, C. L.; Huffman, G. P.; Huggins, F. E. *Nucl. Instrum. Methods* **1984**, *226*, 542−548.

extrapolated spectrum is used in further analysis, which is obtained by logarithmic projection of data points at each energy position to zero time. Data scans were averaged, and a smooth background of a second-order polynomial was removed from the spectrum. Normalization of the data was accomplished by fitting a flattened second-order polynomial to the postedge region and normalizing the fit spline function to 1.0 at 2490 eV. The normalized spectrum of the enedithiolate compound $Na_2S_2C_2H_2$ was subtracted from the spectra of the Ni bis(dithiolene) complexes in order to obtain the pure pre-edge features. Fits to the pre-edges modeled by pseudo-Voigt lines were carried out using the program EDG_FIT[31] with a fixed 1:1 ratio of Lorentzian to Gaussian contributions. The reported intensity values are based on the average of several good fits. In addition to the error resulting from the background correction and fitting procedure (ca. 2%), normalization procedures can introduce ca. 3% error in the total pre-edge peak areas.

C. Electronic Structure Calculations. The base structures of the $[Ni(S_2C_2Me_2)_2]^Z$, $Z = 2-$, $1-$, 0 complex were adopted from their experimental crystal structures[19] by adjusting the atomic coordinates to idealized D_{2h} geometry (Figures S1−S3). Due to asymmetric solid state interactions from the lattice, the actual molecular symmetry in the crystal structure is reduced to C_{2v}; however, it is very close to the D_{2h} point group, within 0.04 Å in Ni−S bond lengths and 0.4° in Ni−S−C bond angles. Other structures used for comparison in this study were obtained from the Cambridge Crystallographic Database.[32]

Density functional calculations were performed using Amsterdam Density Functional 2000[33−36] and Gaussian98[37] packages. As found before,[21,38,39] the use of a triple-ζ basis set with a polarization function (6-311G(d)[40,41] or TZV(d)[42,43] in Gaussian or BSIV[44] in ADF) for the metal and the double-ζ basis set with polarization (6-31G(d)[45,46] in Gaussian, or BSIII[44] in ADF) for the ligand give theoretically converged ground state wave functions. This basis set combination is labeled as BS5 in the Gaussian98 calculations. Because there is only a small increase in computational expense, BSIV was used for all atoms in the ADF calculations.

The adjustment of the amount and type of density functional exchange (DFX) were conveniently achieved using the IOp keywords of the Gaussian98 program. The options 46 and 45 of Overlay 5 were utilized to construct the density functionals from local and nonlocal DF exchange and HF exchange, respectively. The Slater-type local density approximation[47−49] was used, supplemented with the Becke 1988 GGA functional[50] (B88) to define the total DF exchange. The Perdew 1986[51] (P86), Lee−Yand−Parr (LYP),[52,53] PBE and PW91 nonlocal DF correlations were employed with Perdew 1981[54] (P81) and Vosko−Wilk−Nussair[55] (VWN) local DF correlation functionals, respectively. In addition to the commonly used functionals, the asymptotically corrected van Leeuwen−Baerends (LB94[56,57]), Statistical Average of Orbital Potentials(SAOP),[58] Perdew−Burke−Ernzerhof (PBE,[59] PBE98,[60] PBErev[61]) and Perdew−Wang (PW86,[62] PW91[63]) functionals were also utilized.

Single point energy calculations were performed using the tight convergence criterion. In Gaussian98 calculations, population analysis was carried out employing Weinhold's Natural Population Analysis (NPA)[64−66] with the inclusion of the Ni 4p orbitals into the valence set (NPA(4p)). The covalencies of the unoccupied orbitals were calculated as described earlier.[67] In the ADF calculations, the atomic spin densities and the hole covalencies were determined employing Mulliken Population Analysis (MPA).[68]

The hardware used for this study consists of an SGI Origin 2000 8-cpu server, IBM Powerstation 397 workstations, and IBM compatible PCs equipped with 1.0 GHz PIII Xeon and 1.4 GHz Athlon, Athlon 1.9+ MP processors organized into a 50-cpu heterogeneous cluster.

Results and Analyses

1. Transition Dipole Integral: Enedithiolate-S. The sulfur K-edge spectra of Na_2S, $NaSC_2H_5$, and $Na_2S_2C_2H_2$ compounds are shown in Figure 1A. The rising-edge region between 2471 and 2473 eV shows a shift in the edge position to higher energies in the order of sulfide, thiolate, and enedithiolate. This positive energy shift, thus increased energy difference between the S 1s and 4p orbitals, indicates an increase in the sulfur effective nuclear charge (Z_{eff}) in the same order. A linear relationship between the rising-edge position and atomic charge (as well as Z_{eff}) has been derived[69] for a series of compounds, whose charges were determined experimentally from Auger spectroscopy. The S 1s orbital energies directly affect the transition

(31) George, G. N. *EDG_FIT*; Stanford Synchrotron Radiation Laboratory, Stanford Linear Accelerator Center, Stanford University: Stanford, CA.
(32) Allen, F. H.; Kennard, O. *Chemical Design Automation News* **1993**, *8*, 1 and 31−37.
(33) Baerends, E. J.; Ellis, D. E.; Ros, P. *Chem. Phys.* **1973**, *2*, 41−51.
(34) Versluis, L.; Ziegler, T. *J. Chem. Phys.* **1988**, *88*, 322−328.
(35) Te Velde, G.; Baerends, E. J. *J. Comput. Phys.* **1992**, *99*, 84−98.
(36) Guerra, C. F.; Snijders, J. G.; Te Velde, G.; Baerends, E. J. *Theor. Chem. Acc.* **1998**, *99*, 391−403.
(37) Frisch, M. J.; Trucks, G. W.; Schlegel, H. B.; Scuseria, G. E.; Robb, M. A.; Cheeseman, J. R.; Zakrzewski, V. G.; Montgomery, J. A. J.; Stratmann, R. E.; Burant, J. C.; Dapprich, S.; Millam, J. M.; Daniels, A. D.; Kudin, K. N.; Strain, M. C.; Farkas, O.; Tomasi, J.; Barone, V.; Cossi, M.; Cammi, R.; Mennucci, B.; Pomelli, C.; Adamo, C.; Clifford, S.; Ochterski, J.; Petersson, G. A.; Ayala, P. Y.; Cui, Q.; Morokuma, K.; Malick, D. K.; Rabuck, A. D.; Raghavachari, K.; Foresman, J. B.; Cioslowski, J.; Ortiz, J. V.; Stefanov, B. B.; Liu, G.; Liashenko, A.; Piskorz, P.; Komaromi, I.; Gomperts, R.; Martin, R. L.; Fox, D. J.; Keith, T.; Al-Laham, M. A.; Peng, C. Y.; Nanayakkara, A.; Gonzalez, C.; Challacombe, M.; Gill, P. M. W.; Johnson, B.; Chen, W.; Wong, M. W.; Andres, J. L.; Head-Gordon, M.; Replogle, E. S.; Pople, J. A. *Gaussian 98*, revision A.11 ed.; Gaussian, Inc.: Pittsburgh, PA, 1998.
(38) Siegbahn, P. E. M.; Blomberg, M. R. A. *Chem. Rev.* **2000**, *100*, 421−437.
(39) Ryde, U.; Olsson, M. H. M.; Pierloot, K. *Theor. Comput. Chem.* **2001**, *9*, 1−55.
(40) Curtiss, L. A.; McGrath, M. P.; Blaudeau, J.-P.; Davis, N. E.; Binning, R. C. J.; Radom, L. *J. Chem. Phys.* **1995**, *103*, 6104−6113.
(41) McGrath, M. P.; Radom, L. *J. Chem. Phys.* **1991**, *94*, 511−516.
(42) Schaefer, A.; Horn, H.; Ahlrichs, R. *J. Chem. Phys.* **1992**, *97*, 2571−2577.
(43) Schaefer, A.; Huber, C.; Ahlrichs, R. *J. Chem. Phys.* **1994**, *100*, 5829−5835.
(44) Scientific Computing & Modelling NV, S. *Amsterdam Density Functional*, 03 ed.; Vrije Universiteit: Amsterdam, 2000.
(45) Hehre, W. J.; Random, L.; Schleyer, P. v. R.; Pople, J. A. *Ab Initio Molecular Orbital Theory*; Wiley: New York, 1986.
(46) Rassolov, V. A.; Pople, J. A.; Ratner, M. A.; Windus, T. L. *J. Chem. Phys.* **1998**, *109*, 1223−1229.
(47) Hohenberg, P.; Kohn, W. *Phys. Rev.* **1964**, *136*, B864−B871.
(48) Kohn, W.; Sham, L. J. *Phys. Rev.* **1965**, *140*, A1133−A1138.
(49) Slater, J. C. *The Self-Consistent Field for Molecules and Solids. Quantum Theory*.; McGraw-Hill: New York, 1974; Vol. 4.
(50) Becke, A. D. *Phys. Rev. A: Gen. Phys.* **1988**, *38*, 3098−3100.
(51) Perdew, J. P. *Phys. Rev. B: Condens. Matter* **1986**, *33*, 8822−8824.
(52) Lee, C.; Yang, W.; Parr, R. G. *Phys. Rev. B: Condens. Matter* **1988**, *37*, 785−789.
(53) Miehlich, B.; Savin, A.; Stoll, H.; Preuss, H. *Chem. Phys. Lett.* **1989**, *157*, 200−206.
(54) Perdew, J. P.; Zunger, A. *Phys. Rev. B: Condens. Matter* **1981**, *23*, 5048−5079.
(55) Vosko, S. H.; Wilk, L.; Nusair, M. *Can. J. Phys.* **1980**, *58*, 1200−11.
(56) van Leeuwen, R.; Baerends, E. J. *Phys. Rev. A* **1994**, *49*, 2421−2431.
(57) Grüning, M.; Gritsenko, O. V.; van Gisbergen, S. J. A.; Baerends, E. J. *J. Chem. Phys.* **2001**, *114*, 652−660.
(58) Schipper, P. R. T.; Gritsenko, O. V.; van Gisbergen, S. J. A.; Baerends, E. J. *J. Comput. Phys.* **2000**, *112*, 1344−1352.
(59) Perdew, J. P.; Burke, K.; Ernzerhof, M. *Phys. Rev. Lett.* **1996**, *77*, 3865−3868.
(60) Zhang, Y. K.; Yang, W. T. *Phys. Rev. Lett.* **1998**, *80*, 890.
(61) Hammer, B.; Hansen, L. B.; Norskov, J. K. *Phys. Rev. B: Condens. Matter* **1999**, *59*, 7413−7421.
(62) Perdew, J. P.; Wang, Y. *Phys. Rev. B: Condens. Matter* **1986**, *33*, 8800−8802.
(63) Perdew, J. P.; Chevary, J. A.; Vosko, S. H.; Jackson, K. A.; Pederson, M. R.; Singh, D. J.; Fiolhais, C. *Phys. Rev. B: Condens. Matter* **1992**, *46*, 6671−6687.
(64) Foster, J. P.; Weinhold, F. *J. Am. Chem. Soc.* **1980**, *102*, 7211−7218.
(65) Carpenter, J. E.; Weinhold, F. *THEOCHEM* **1988**, *169*, 41−62.
(66) Reed, A. E.; Curtiss, L. A.; Weinhold, F. *Chem. Rev.* **1988**, *88*, 899−926.
(67) DeBeer George, S.; Metz, M.; Szilagyi, R. K.; Wang, H.; Cramer, S. P.; Lu, Y.; Tolman, W. B.; Hedman, B.; Hodgson, K. O.; Solomon, E. I. *J. Am. Chem. Soc.* **2001**, *123*, 5757−5767.
(68) Mulliken, R. S. *J. Chem. Phys.* **1955**, *23*, 1833−1840.
(69) Shadle, S. E.; Hedman, B.; Hodgson, K. O.; Solomon, E. I. *J. Am. Chem. Soc.* **1995**, *117*, 2259−2272.

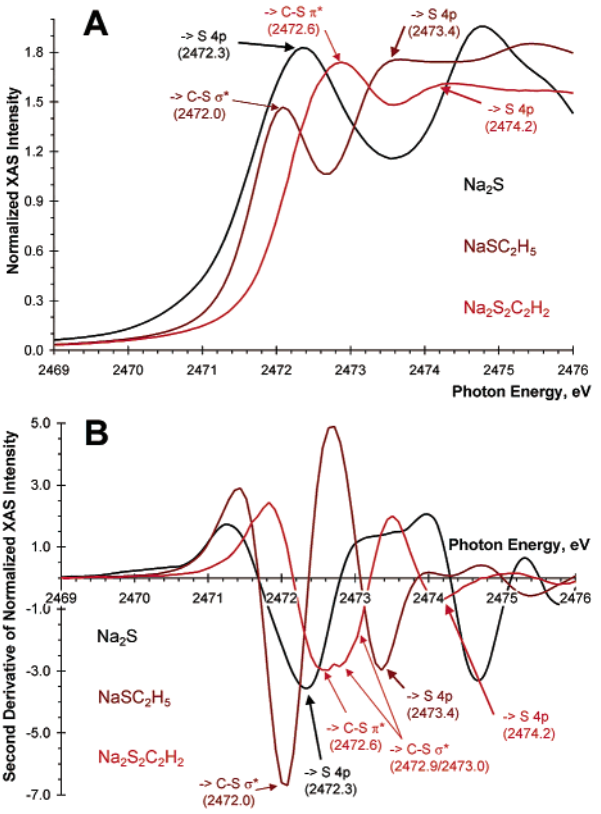

Figure 1. Sulfur K-edge spectra (A) and second derivatives (B) of sulfide (black line), thiolate (brown line), and enedithiolate (orange line) sodium salts (energies in parenthesis are given in eV).

dipole integral I(S 1s→3p). The dipole integral has already been evaluated for sulfide ($I(S^s) = 6.54$)[70] and thiolate ($I(S^t) = 8.05$)[71] ligands, respectively, and increases with increasing Z_{eff}. The increase in the edge energy position and thus further increase in the Z_{eff} of the S atom in the enedithiolate indicate the necessity to derive a new transition dipole integral for an enedithiolate-S.

In Figure 1B, a reasonable assignment is given for the rising-edge region based on the minimum positions of the second derivatives. Using the molecular orbital description of the free ligands (*vide infra*), the S 1s→C−S π*, 1s→C−S σ*, and 1s→4p transitions can be assigned as indicated. This assignment gives an approximately linear increase of the S 1s→4p transition energies going from sulfide to thiolate (+1.1 eV) and from thiolate to enedithiolate (+0.8 eV). This linear trend is supported by calculated changes in the S atomic charges, S 1s orbital energies, and S 1s→4p transition energies (see Supporting Information, Table S1) for the organic ligands with geometry optimized sodium ion positions.

The approximate S 1s→4p transition energies, given in parentheses in Figure 1A and B, were used to estimate changes in Z_{eff} and thus determine the transition dipole integral ($I(S^e)$) for enedithiolate-S. A change of +1.1 eV in the S 1s→4p energy between sulfide and thiolate corresponds to a +1.51 increase in the transition dipole integral. The corresponding transition in the enedithiolate salt is 0.8 eV higher than the thiolate, which

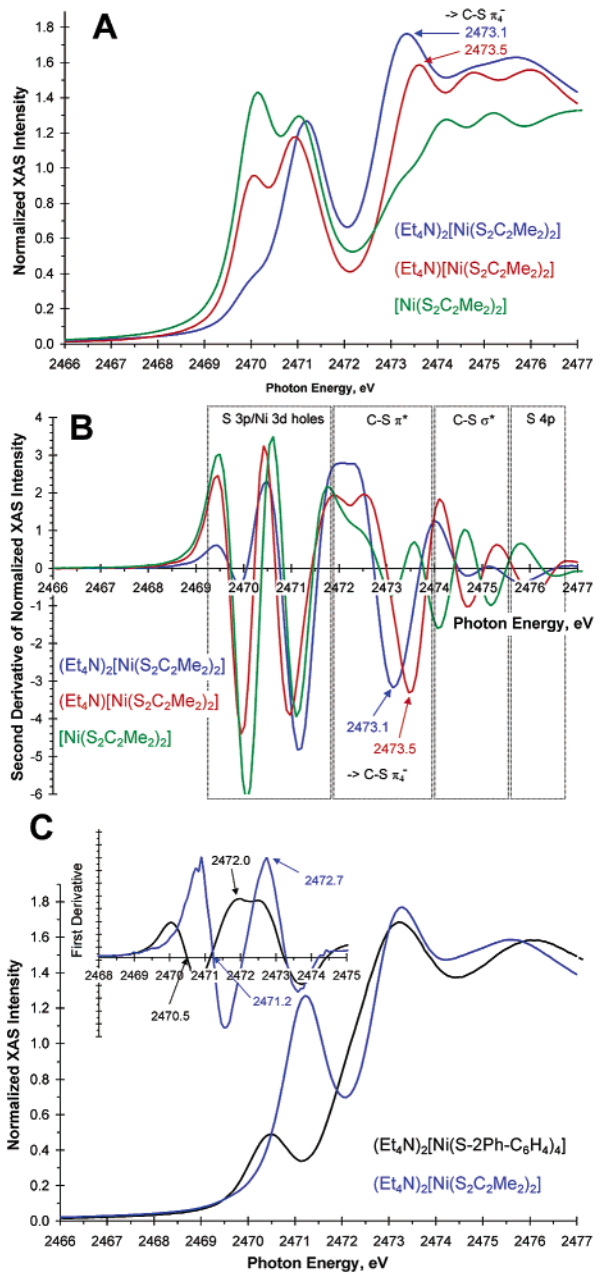

Figure 2. Sulfur K-edge spectra (A) and second derivatives (B) of $(Et_4N)_2$-$[Ni(S_2C_2Me_2)_2]$ (blue line), $(Et_4N)[Ni(S_2C_2Me_2)_2]$ (red line), and $[Ni(S_2C_2Me_2)_2]$ (green line) compounds (energies are given in eV). The spectrum of $(Et_4N)_2[Ni(S\text{-}2Ph\text{-}C_6H_4)_4]$ (black line, adapted from ref 2) and the contamination corrected spectrum of $(Et_4N)_2[Ni(S_2C_2Me_2)_2]$ are shown in part C with their first derivatives as the inset.

reflects the different covalent bonding due to delocalization of S electron density into the C π-system, and gives a value of 9.15 for $I(S^e)$. As will be developed below, this integral will need to be further increased for the Ni bis(dithiolene) complexes, since there is significant electron donation from the dithiolene ligand to the metal, which further increases the Z_{eff} of the enedithiolate-S in the complex.

2. Quantitation of Ground State Covalencies: $[Ni(S_2C_2Me_2)_2]^Z$, $Z = 2-, 1-, 0$. 2.1. Sulfur K-Edge Spectra. Figure 2A shows the pre-edge (2469−2472 eV) and rising-edge (2472−2475 eV) regions of the S K-edge spectra of the Ni bis-(dithiolene) series. In general, the edge positions shift to higher energy in going from the dianionic to the neutral complexes.

(70) Rose, K.; Shadle, S. E.; Glaser, T.; de Vries, S.; Cherepanow, A.; Canters, G. W.; Hedman, B.; Hodgson, K. O.; Solomon, E. I. *J. Am. Chem. Soc.* **1999**, *121*, 2353−2363.
(71) Shadle, S. E.; Penner-Hahn, J. E.; Schugar, H. J.; Hedman, B.; Hodgson, K. O.; Solomon, E. I. *J. Am. Chem. Soc.* **1993**, *115*, 767−776.

Table 1. Pre-edge Peak Energies (E, eV), Intensities (D_0, −), Ground State Degeneracy (A, −), Transition Dipole Integrals of Ni Bound Dithiolene Sulfur (I(S), −) and Covalencies (α^2, %) of S K-edge Data for $[Ni(S_2C_2Me_2)_2]^Z$ Complexes

Z	E, eV	D_0	A	I(S)	$\alpha^{2\,a}$	$\overline{\alpha^{2}}^{b}$	$\overline{\alpha^{2}\cdot A}^{c}$
2−	2471.2	1.3238	2	9.84	81	77	77
1−	2470.0	0.5390	1	10.39	62	59	67
	2471.0	1.2945	2		75	71	
0	2470.1	1.2768	2	10.94	70	67	62
	2471.1	1.0890	2		60	57	

[a] Quantitation was based on the expression $D_0 = (A/3n)\alpha^2 I(S)$, where n is the normalization factor (i.e., number of S atoms contributing to the pre-edge feature, $n = 4$ for Ni bis(dithiolene) complexes). [b] XAS and EPR covalency values averaged for the $Z = 1-$ complex, used for comparisons to DFT calculations. [c] Hole-weighted averages.

The change in the Z_{eff} of the S atom in the complexes can be correlated with the shift in the S 1s→C−S π_4^* transitions (indicated by arrows in Figure 2A and B) for the di- (2473.1 eV) and monoanionic complexes (2473.5 eV). In the case of the neutral complex, the structure of the rising edge changes drastically. Based on the very similar change in pre-edge intensities (*vide infra*) between the monoanionic and the neutral forms relative to the di- and monoanionic forms, the edge position is expected to shift similarly by 0.4 eV to higher energies.

The S 1s→C−S π_4^* transitions (Figure 2) of the dianionic (2473.1 eV), monoanionic (2473.5 eV) and netural (approximately 2473.9 eV) complexes can be correlated with the S 1s→π_4 transition of free enedithiolate salt (2472.6 eV, Figure 1) to estimate the transition dipole integral I(S) for the dithiolene sulfur ligand in the Ni complexes, which correspond to 0.69, 1.24, and 1.79 increases, respectively, relative to $I(S^e)$ of the enedithiolate salt. The Z_{eff} corrected transition dipole integrals for the Ni bound dithiolene sulfur ligands are summarized in Table 1.

However, the pre-edge features do not change their energy positions significantly, which is strikingly different from the behavior observed for the pre-edge energy positions of the ferrous/ferric tetrachlorides[69] and tetrathiolates.[2,72] The edge energy positions of the ferrous and ferric complexes shift up by 1.0 eV in the chloride and by 0.5 eV in the thiolate complexes indicating increasing Z_{eff} (and decreasing core 1s orbital energies) of the Cl and S atoms upon oxidation of the complex. However, the pre-edge energy positions show the opposite trend, since they are 2.0 and 1.0 eV lower for the Fe^{III} chloride and thiolate complexes, respectively, than those for the corresponding Fe^{II} complexes. In general, the pre-edge energy position is determined by the energy of the metal d-manifold and the S/Cl core 1s orbital. By correcting the pre-edge shifts with the shift in the edge energies, the d-manifold stabilizations are estimated to be 3.0 and 1.5 eV for the chloride and thiolate complexes going from Fe^{II} to Fe^{III}. The smaller d-manifold stabilization in the thiolate complexes upon oxidation is due to its more covalent bonding relative to the chloride complexes. In the case of the Ni bis(dithiolene) complexes, the shift in the rising-edge position gives the decrease of the S 1s orbital energies (i.e., the increase of Z_{eff} for S) to be only 0.4 eV between the di- and monoanionic complexes and approximately the same between the monoanionic and neutral complexes. The constant energy position of the pre-edge features requires a similarly constant compensation of the d-manifold energy. The smaller change in the d-manifold of the Ni dithiolenes (0.4 eV) compared to that of the thiolate complexes (1.5 eV) indicates a smaller change in Z_{eff} on the metal atom, arguing for larger ligand characters in the Ni dithiolene complexes. In addition, this indicates that oxidation of the Ni dithiolene complexes mainly occurs on the ligand. The approximately 0.4 eV stabilization of the d-manifold of the Ni atom (i.e., a small change in the Ni Z_{eff}) upon oxidation is also observed in metal K-edge data (see Supporting Information, Figure S7) from the small shift (0.5 eV) of the direct Ni 1s→4p transition energies. It is also worth noting that, in the Ni K-edge spectra of the Ni bis(dithiolene) complexes (Figure S7), the pre-edge features around 8832 eV, which are the quadrupole allowed, Ni 1s→3d transitions, have very little intensity. Alternatively, the Ni^{II} thiolate has a factor of 2 to 3 more pre-edge intensity at the Ni K-edge, which is due to the Ni 4p mixing into the Ni 3d orbitals giving an electric dipole allowed Ni 1s→4p transition in a tetrahedral, noncentrosymmetric structure.

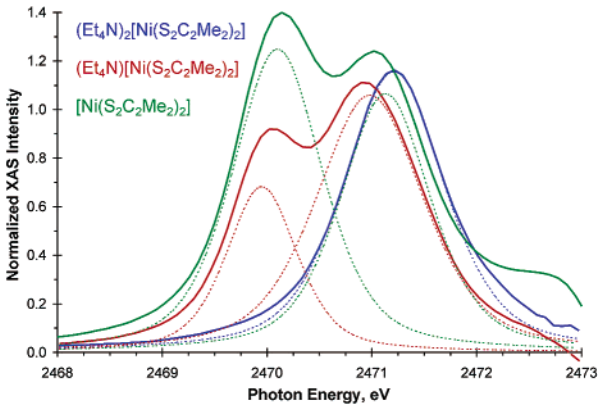

Figure 3. Representative fits of the pre-edge features of the Ni bis(dithiolene) series (background subtractions using S K-edge spectrum of $Na_2S_2C_2H_2$ shifted by +0.5 eV, +0.8 eV, and +1.1 eV for $Z = 2-$, $1-$, and 0, respectively).

In Figure 2A, the spectra of the monoanionic and the neutral complexes show two pre-edge features split by 1 eV. The dianionic complex shows one pre-edge feature with a small shoulder on the low energy side. The energy position of the main pre-edge feature aligns well with the high energy feature of the monoanionic and the neutral forms. The dianionic complex is known to be highly air-sensitive, and in addition, its spectrum changes with time in the beam (slow photoreduction). The low energy shoulder corresponds to a contamination from the oxidized form, which also shows up in the EPR spectrum of the measured sample. The concentration of the impurity cannot be analytically determined by EPR spin quantitation due to the inherent limitation of sample recovery after XAS data collection.

Figure 3 shows the background subtracted data and representative fits for the Ni dithiolene complexes. Table 1 summarizes the pre-edge energy positions and intensities. The details of each fit are given in Supporting Information (Figures S4−S6). For background correction, the S K-edge spectrum of the $Na_2S_2C_2H_2$ compound shifted by +0.5, +0.8, and +1.1 eV was subtracted from the spectra of the Ni complexes minimizing the residuals above 2473 eV. The equal spacing of the shifts in

(72) Rose, K.; Shadle, S. E.; Eidsness, M. K.; Kurtz, D. M. J.; Scott, R. A.; Hedman, B.; Hodgson, K. O.; Solomon, E. I. *J. Am. Chem. Soc.* **1998**, *120*, 10743−10747.

the background correction is an additional indication of the equal change in the Z_{eff} of the dithiolene sulfur in going from the di- to monoanionic and to the neutral compound (*vide supra*). Scaling the ligand salt spectra to best fit the rising edge of the Ni complex spectra gave identical background corrected pre-edge features within 1%. To account for the impurity in the spectrum of the dianionic complex, 20% of the background-corrected monoanionic spectrum was subtracted to eliminate the low energy shoulder at 2470.0 eV followed by renormalization with a factor of 1/0.8 (Figure 2C). The fitting procedure using equally mixed Lorentzian/Gaussian functions gave total pre-edge intensities of 1.32, 1.83, and 2.37 (Figures S4−S6) for $Z = 2-$, $1-$, and 0, respectively. These give approximately equal intensities for each of the transitions (ca. 0.6), assuming two, three, and four S 1s→φ* transitions for the di-, monoanionic, and neutral complexes, respectively.

The use of fixed line widths gave good fits for the dianionic and neutral forms (Figures S4 and S6). The pre-edge intensity of the dianionic form corresponds to 81% S 3p character (α^2), while, for the neutral form, the high- and low-energy pre-edge features give 60% and 70%, respectively. For the monoanionic form, the line width of the higher energy feature had to be increased by 0.2 eV (Figure S5) to account for multiplet effects associated with the 1-electron excited $(b_{2g})^1(b_{1g})^1$ configuration (*vide infra*), which gives $^3B_{3g}(\alpha 5b_{2g} \times \alpha 13b_{1g})$ and $^1A_g(\alpha 5b_{2g} \times \beta 5b_{2g})$ d^{n+1}-parent states. The intensities of the low- and high-energy features in the monoanionic form give covalencies of 62% and 75%, respectively. The ligand character (62 ± 5%) of the SOMO (*vide infra*) in this paramagnetic species fits reasonably well with the EPR spin density[73] of 55 ± 5% demonstrating the complimentarity of the two independent techniques. This further supports the transition dipole integral determined from correlation of the S 1s→π_4 and 1s→π_4^- transitions of the Na salt of the enedithiolate compound and the Ni bis(dithiolene) complexes.

As a reference, Figure 2C also includes the S K-edge spectra of the $(Et_4N)_2[Ni(S\text{-}2Ph\text{-}C_6H_4)_4]$ complex with a distorted tetrahedral coordination geometry of the central Ni^{II} atom. The ground state of this complex is a triplet with two singly occupied-orbitals of the t_2-set. The S K-edge spectrum shows the doubly degenerate S 1s→ψ*(t_2) transition at 2470.5 eV. The ground state covalency was determined to be 33% S 3p character[2] for each of the t_2-holes. The comparison of the square-planar bis(dithiolene) and tetrahedral tetrathiolate Ni^{II} complexes reflects both effects of the different coordination geometries of the central Ni atom and the different chemical natures of the ligands. The rising-edge inflection point (first maximum of the first derivative spectrum) shifts to higher energies in the Ni bis-(dithiolene) complex by approximately 0.7 eV (inset of Figure 2C, 2472.0 to 2472.7 eV), which correlates well with the shift in the S 1s→C−S σ* and 1s→C−S π* energies of the sodium salts of the thiolate and enedithiolate ligands (0.6 eV, Figure 1A, 2472.0 to 2472.6 eV), respectively. The pre-edge feature also shifts up in energy by approximately 0.7 eV, which implies essentially no change in the d-orbital energy, which is opposite what is generally expected in going from a tetrahedral to a square-planar coordination geometry. The constant energy of the acceptor d-orbital and the nearly 2-fold increase in the pre-edge intensity indicate a significantly more covalent bond in the square-planar dithiolene complex, even taking into account the 22% increase in the dithiolene-S transition dipole integral relative to that of the thiolate-S.

As quantified in Table 1, the S 3p ligand character of the low energy pre-edge feature increases going from the monoanionic form (62%) to the neutral complex (70%), while that of the high-energy pre-edge feature decreases from 81% in the dianionic form to 60% in the neutral complex. In all cases, the covalency is above 50%. This means that, upon oxidation of the dianionic and the monoanionic forms, more than 50% of the electron density is lost from an S based orbital, which is consistent with the constant pre-edge energies and changes in intensities. The total ligand character is, in fact, larger due to the non-negligible C and H contributions (10−20%) of the dithiolene fragment to these orbitals.

The final experimental covalency values of the Ni bis-(dithiolene) series have been obtained by averaging the EPR spin distribution[8,11,12] and the S K-edge XAS covalencies (results from two independent experimental techniques, Table 1, $\overline{\alpha^2}$). These values are used to correlate experiment to DFT calculations.

2.2. Density Functional Calculations. 2.2.1. Enedithiolate Ligand. The MO diagram for $[S_2C_2Me_2]^{2-}$ obtained from BP86/BS5 DFT calculations is presented in Figure 4A. Due to the C_{2v} symmetry of the free ligand, the MOs can be divided into out-of-plane (π, along the *z*-axis, a_2 and b_1) and in-plane (σ, in the xy-plane, a_1 and b_2) orbitals. The four π-orbitals are best described by a butadiene-like π-system with π_1, π_2, π_3 double-occupied and π_4 (or π*) unoccupied. The HOMO of the enedithiolate ligand is the negative combination (σ_-) of S $3p_x+3p_y$ orbitals, while the positive combination (σ_+) is at slightly lower energy than π_2. The two highest occupied MOs (σ_- and π_3) have mainly S 3p character and are important in bonding to Ni in the dithiolene complexes. These frontier orbitals are at high energy due to in-plane S···S and out-of-plane S−C antibonding interactions, which are caused by the constrained enedithiolate geometry.

Figure 4B includes two enedithiolate ligands to account for ligand-ligand repulsion induced orbital splitting. They are located relative to each other as in the experimental structure of the $(Et_4N)_2[Ni(S_2C_2Me_2)_2]$ complex at an S···S interligand distance of 3.1 Å, but without the Ni atom. The positive and negative combinations of π_4 orbital remain in the virtual orbital space for the pure ligand system in Figure 4B and for the Ni complexes. Their energies do not change significantly (by at most 0.05 eV) upon variation in interligand distances along the Ni bis(dithiolene) series. It is notable that while the π_4^+ orbital of the ligand system can in principle participate in a back-bonding interaction with the Ni $3d_{yz}$ orbital, it has only limited S character (<10%). However, the HOMO(σ_-) of the hypothetical bis(enedithiolate) ligand system can strongly interact with the LUMO($3d_{xy}$) of the Ni^{II} ion in a square-planar ligand field. The next lower orbital is the negative combination of the two π_3 orbitals, which can have an antibonding overlap with the Ni $3d_{xz}$ orbital. Lower lying bis(enedithiolate) orbitals

(73) The EPR *g*-values and parallel hyperfine coupling constants are slightly different for $[Ni(S_2C_2(CN)_2)_2]^{1-}$ and $[Ni(S_2C_2Me_2)_2]^{1-}$, with a large error bar for the perpendicular hyperfine coupling constant of the latter complex. This uncertainty introduces 15% error in the quantitation of the S spin densities (47%-69% S 3p and 1−2% S 3s character) of the methyl derivative. However, gradient corrected density functional calculations indicate quantitatively similar ground state descriptions, and therefore, the value and error bars obtained for the maleonitrile complex is used.

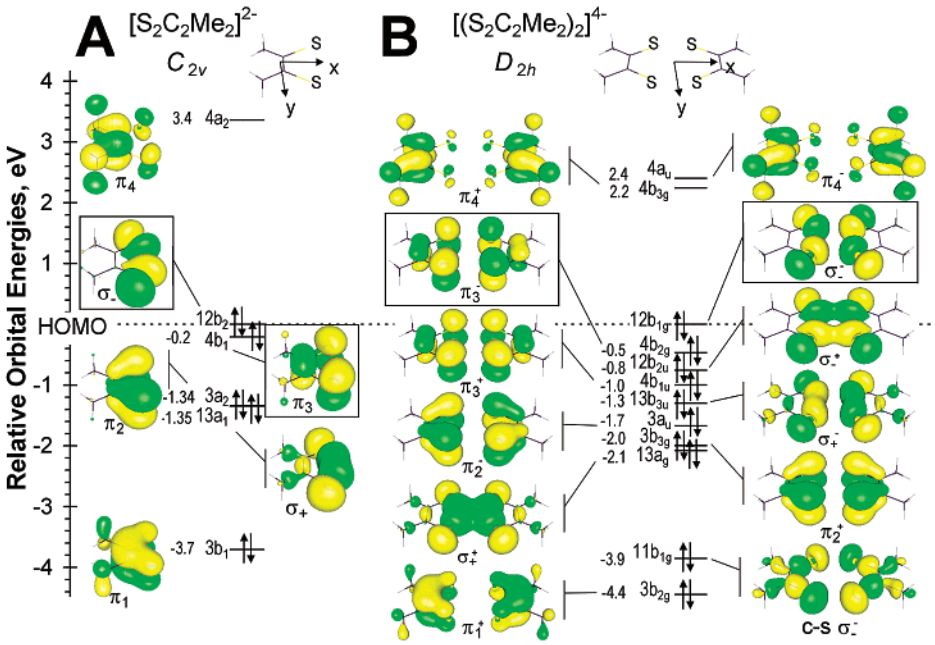

Figure 4. Kohn−Sham orbital picture of the mono- (A) and bis(enedithiolate) (B) ligands with symmetrized geometry from the X-ray structure of $(Et_4N)_2[Ni(S_2C_2Me_2)_2]$ calculated at the B88P86/BS2 level (subscripts +/− refer to in-/out-of-phase combinations of S 3p orbitals within one enedithiolate; superscripts +/− refer to a combination between two enedithiolates).

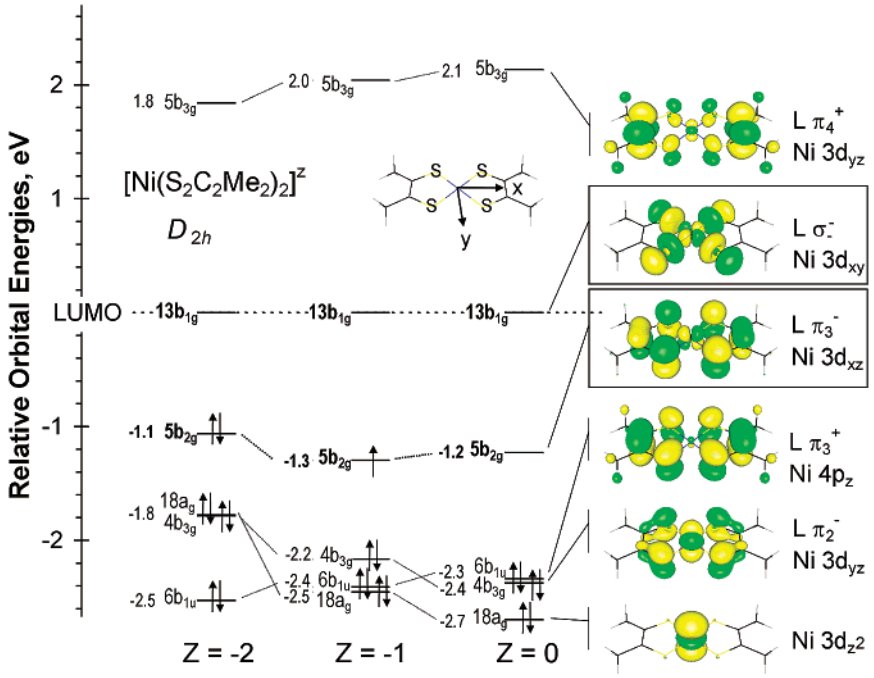

Figure 5. Kohn−Sham orbital picture of the Ni bis(dithiolene) series with symmetrized geometry from the X-ray structure of $[Ni(S_2C_2Me_2)_2]$ calculated at the B88P86/BS5 level.

including the σ_-^+ and π_3^+ orbitals, which can mix with the Ni $4p_y$ and $4p_z$ orbitals, are also presented in Figure 4B for reference; however, they do not contribute to the levels probed by S K-edge XAS.

2.2.2. Ni Bis(dithiolene) Complexes. The orbital energy levels calculated using B88P86/BS5 of the three Ni bis(dithiolene) complexes are presented in Figure 5. Since the orbital contour plots qualitatively do not change along the series, they are only given for the neutral complex. The ligand S 3p characters calculated by using B88 density functional exchange (DFX) and P86 density functional correlation (DFC) functionals with various mixing of Hartree−Fock exchange (HFX) are summarized in Table 2. Based on a systematic basis set and population analysis calibration (summarized in Supporting Information, Table S2), the BS5 (triple-ζ plus single polarization functional on the metal and double-ζ plus polarization on the ligand) was found to give a theoretically converged ground state description. The covalencies are determined by means of Weinhold's Natural Population Analysis (NPA) including the Ni 4p atomic orbital into the valence set.

2.2.2.1. $[Ni(S_2C_2Me_2)_2]^{2-}$ Complex. The LUMO of the dianionic complex ($13b_{1g}$ in Figure 5) is the antibonding

Table 2. Calculated Ground State S 3p Covalencies (%) of the Experimentally Probed LUMO and LUMO+1 Orbitals for the Ni Bis(dithiolene) Series and Spin Densities (in electron, including C and H Contributions) on Each of the Dithiolene Ligands by Means of NPA(4p) at the B88P86/BS5 Level

Spin Restricted Wave Functions								
HF exchange →		0%	10%	20%	25%	50%	100%	pure HF
$Z = 2-$	$13b_{1g}$	53	51	46		35	18	12
$Z = 1-$	$5b_{2g}$	60	59	62		69	70	74
	$13b_{1g}$	58	56	53		41	22	21
$Z = 0$	$5b_{2g}$	62	62	63	64	65	66	65
	$13b_{1g}$	59	57	54	52	43	24	23
Spin Unrestricted Wave Functions								
HF exchange →		0%	10%	20%	25%	50%	100%	pure HF
$Z = 1-$	β-$5b_{2g}$	60	60	61		68	71	71
	α-$13b_{1g}$	59	56	54		42	22	20
	β-$13b_{1g}$	56	53	48		30	5	1
	$\langle S^2 \rangle$	0.7515	0.7532	0.7557		0.7630	0.7825	0.7893
ligand spin density		0.39	0.39	0.39		0.47	0.54	0.55
$Z = 0$	$5b_{2g}$	62	62	63	63	58	49	
	$13b_{1g}$	59	57	54	52	41	24	
	$\langle S^2 \rangle$	0.0000	0.0000	0.0000	0.1817	0.7752	0.9811	
ligand spin density[a]		0.0	0.0	0.0	±0.43	±0.88	±0.99	

[a] ± sign indicates opposite spin on each dithiolene ligand.

combination of the Ni $3d_{xy}$ and ligand σ_-^- orbitals. Due to the ligand geometry, the overlap between these two orbitals is highly favorable, providing an efficient pathway for ligand-to-metal electron donation, that is, a highly covalent bond. The HOMO is an out-of-plane orbital with Ni $3d_{xz}$ and ligand π_3^- fragment orbitals. Based on the orbital contour plots shown in Figure 5, the frontier orbitals of the complexes have mainly S ligand character in good agreement with the pre-edge data. In terms of quantitative comparison (Table 2, top), the B88P86 calculation gives a ground state description with less ligand character in the LUMO (53%) than the value estimated from the pre-edge data (77%) using the Z_{eff} corrected transition dipole integral (vide supra). The gradient-corrected (GGA) density functional calculations generally give too much ligand character for late transition metals as found for Cu^{II} complexes.[21] In the case of Ni bis(dithiolene) complexes, mixing of HFX gradually gives less ligand character in worse agreement with experiment. The effect of using different local and nonlocal DFX and DFC functionals has been evaluated, and the results are given in the Supporting Information (Table S3). Change in LDA and DFC functionals did not affect significantly the ground state covalencies. The functional based on the statistical average of orbital potentials[58] gave 4% more S character than the common GGA functionals, which was increased further to 63% by using the van Leeuwen−Baerends functional (LB94).[56,57] Thus, the LB94 functional gives the most reasonable description of the experimental ground state for the dianion complex,[74] but still with too little ligand character.

2.2.2.2. $[Ni(S_2C_2Me_2)_2]^{1-}$ Complex. Oxidation of the dianionic complex creates a hole in the out-of-plane SOMO ($5b_{2g}$), which is the antibonding combination of the Ni $3d_{xz}$ and ligand π_3^- fragment orbitals (Figure 5). The LUMO remains the in-plane $13b_{1g}$ orbital, which is very similar to the LUMO of the dianionic complex. Experimentally (Figure 3 and Table 1), we observe a decrease of the LUMO covalency from 77 to 71%. The GGA density functional calculations using B88P86 give an excellent description of the SOMO within 1% of S 3p character but with a reverse SOMO to LUMO covalency ratio (1.03, Table 2, top) compared to experiment (0.83). Hybrid functionals do not improve the calculated ground state description compared to experiment. Increasing the amount of HFX decreases the ligand character of the in-plane orbital ($13b_{1g}$) and increases that of the out-of-plane orbital ($5b_{2g}$). The LB94 and SAOP functionals, giving more covalent bonding (vide supra), increase the covalency in both orbitals (Table S4) slightly improving the overall agreement with data. Spin-unrestricted calculations were also performed to take into account spin polarization, which did not give significantly different covalencies for the GGA density functional calculation (Table 2, bottom). The unrestricted spin-density contour plot is practically identical to the SOMO of the spin-restricted calculation. The spin-unrestricted hybrid calculations increase the spin polarization of the wave function, as can be seen from the increasing deviation of the spin expectation values ($\langle S^2 \rangle$) from the ideal value of 0.7500. The increased spin polarization, which is due to higher spin state contamination, changes the $\alpha 13b_{1g}$ (αLUMO) orbital relative to the $\beta 13b_{1g}$ (βLUMO+1) level (Table 2, bottom). The spin density on each of the dithiolene ligands in spin-unrestricted calculations increases from 0.39 to 0.55 as the amount of HF exchange increases to 100%, showing more ligand character than in the experimental results (approximately 0.30 S + 0.05 αC per dithiolene ligand based on EPR/ENDOR/ESEEM total atomic spin distributions[12]).

Among the available pure and hybrid density functionals, the common GGA functionals (such as B88P86 or B88LYP) give the closest agreement with the experimental covalencies of the monoanionic complex with a negligible difference between the spin-restricted and unrestricted wave functions.

2.2.2.3. $[Ni(S_2C_2Me_2)_2]$ Complex. The qualitative description of the two lowest unoccupied MOs of the neutral complex in the Ni bis(dithiolene) series is very similar to those of the mono- and dianionic complexes. The energy difference between the

(74) As an alternative method, adjustment of the Ni Z_{eff} to stabilize the d-manifold relative to the dithiolene ligand orbitals can be achieved by increasing the Ni nuclear charge by half electron, which gives Ni 3d and S 3p characters of the $13b_{1g}$ hole in the dianion complex of 32% and 65%, respectively, at BP86/BSIV level of theory by means of Mulliken Population Analysis.

LUMO($5b_{2g}$) and LUMO+1($13b_{1g}$) orbitals (1.2 eV) does not change significantly relative to the monoanionic complex (1.3 eV), which is consistent with the experimental pre-edge results in Figure 2. The energy difference between the S pre-edge peaks of the monoanionic and neutral species is slightly larger than 1.0 eV (Table 1, Figures S5 and S6). The calculated ground state description at B88P86/BS5 level (Table 2, top, first column) gives a reasonable estimate of the covalencies (62% and 59%) in comparison to experimental values (67% and 57% S 3p character in $5b_{2g}$ and $13b_{1g}$ levels, respectively). Inclusion of HFX provides improvement in the $13b_{1g}$ orbital covalencies. Mixing of 10% HFX gives a good fit to experimental orbital covalencies. The spin polarization of the wave function (Table 2, bottom) has also been evaluated using the broken symmetry formalism within C_{2v} symmetry. In these spin-unrestricted calculations, the covalent, ground state wave function was taken as a reference point and the linear combinations of the HOMO ($6b_{1u}$) and LUMO ($5b_{2g}$) were taken as the initial guess ($10b_2$ and $11b_2$ in C_{2v}, respectively). The positive combination of these two orbitals was used for the occupied α-set, while the negative combination was occupied in the β-set introducing initial spin polarization. The electron density for the lowered symmetry (C_{2v} wave function on a D_{2h} nuclear framework) was optimized within the SCF procedure. The GGA and hybrid density functional calculations with up to 20% HFX (the B3LYP approximation[75]) give a delocalized, covalent ground state with zero atomic spin densities. A gradual increase of HFX mixing above 20% results in some localization of the broken symmetry wave functions ($\langle S^2 \rangle \neq 0$) with a continuous increase of spin polarization from 22% HFX mixing (Figure 6A). For 25% and 50% HFX, approximately 0.4e and 0.9e spin density are present on each dithiolene ligand with opposite sign (see Figure 6B and C, respectively).

On the basis of the comparison of the experimental S 3p covalencies of the neutral complex with those of the calculated wave functions, a hybrid functional with 10% HFX mixing properly describes the ground state of the neutral complex. Alternatively, if the lower limit of the ligand covalency is used (based on the EPR spin distribution), the data require inclusion of approximately 25% HFX. Density functionals calibrated to fit XAS data lead to no spin polarization, while functionals calibrated to fit EPR data give some spin polarization with up to 0.4 of an electron spin on each of the ligands. In the latter limit, the metal (ca. 25% Ni $3d_{xz}$ in $5b_{2g}$ in Figure 5) acts as a superexchange pathway between the two partially spin polarized dithiolene ligands.

Discussion

As developed above, the $13b_{1g}$ and $5b_{2g}$ orbitals (Figure 5) are important in describing the bonding in the $[Ni(S_2C_2Me_2)_2]^Z$, $Z = 2-$, $1-$, and 0 series. The $13b_{1g}$ orbital (antibonding combination of Ni $3d_{xy}$ and the bis(dithiolene) σ^- orbitals) is at higher energy than the $5b_{2g}$ orbital (antibonding combination of Ni $3d_{xz}$ and bis(dithiolene) π_3^- orbitals). The corresponding pre-edge features of the S K-edge XAS spectra in Figure 3 are the peaks at 2470 and 2471 eV, respectively. The Ni $3d_{yz}$ orbital has a small antibonding interaction with the bis(dithiolene) π_4^+ orbital ($5b_{3g}$ in Figure 5), which can be seen experimentally by XAS for the neutral complex at around 2473 eV at the rising S K-edge (Figure 2). Other than this contribution, which is negligible in terms of bonding, the remaining three Ni d-orbitals either do not interact with ligand orbitals ($3d_{z^2}$ and $3d_{x^2-y^2}$) or their bonding and antibonding combinations are occupied ($3d_{yz}$) in all three complexes. The S K-edge XAS pre-edge intensities indicate dominant S character in both unoccupied orbitals. This is due to the strong ligand−ligand repulsion derived from the short S···S distances, which is the consequence of the constrained αC−αC bond of the enedithiolate. The more than 50% ligand character in the ground state wave function indicates an inverted bonding scheme[76] with destabilized ligand orbitals relative to the d-manifold. In the case of an inverted bonding scheme (Scheme 1B), a decrease of the ligand character ($1 - \alpha^2$) corresponds to a more covalent bond, which is opposite to that of a normal bonding description (Scheme 1A, *vide supra*).

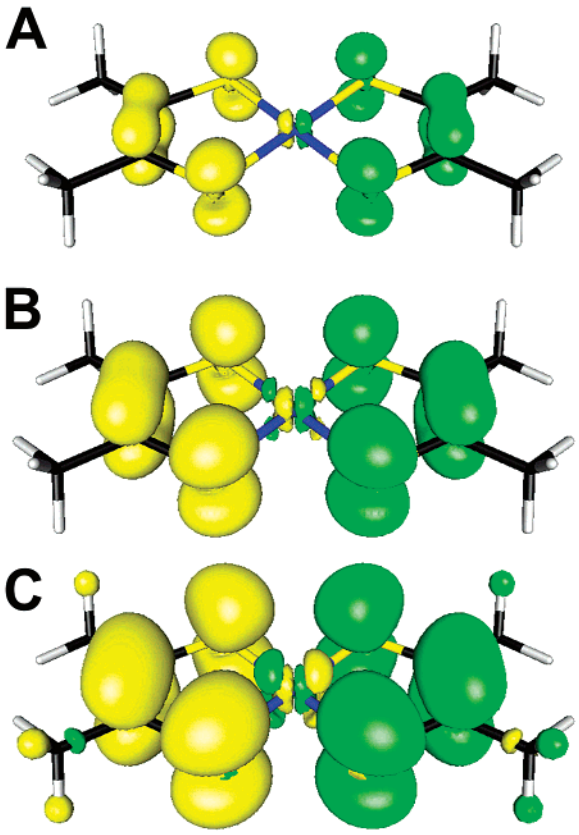

Figure 6. Spin-density contour plots of the localized, broken symmetry wave functions for $[Ni(S_2C_2Me_2)_2]$ at B88(22HF)P86/BS5 (A), B88(25HF)-P86/BS5 (B), and B88(50HF)P86/BS5 (C) levels of theory.

The ligand covalencies of the two redox active orbitals ($13b_{1g}$ at 2470 eV and $5b_{2g}$ at 2471 eV, Table 1) show a systematic trend along the series. The experimental S 3p character of the $13b_{1g}$ orbital is the highest (77%) in the dianionic complex, which decreases by 6% in the monoanionic and an additional 14% in the neutral complex. The opposite behavior is observed for the out-of-plane $5b_{2g}$ orbital contributions for the monoanionic (59%) and the neutral complexes (67%).[77] Overall, the hole-weighted S character ($\overline{\alpha^2} \cdot A$, Table 1) decreases with oxidation. This is opposite to what has been observed for the tetrachloride and thiolate complexes, where the ligand character

(75) Becke, A. D. *J. Chem. Phys.* **1993**, *98*, 5648−5652.

(76) Li, J.; Noodleman, L.; Case, D. A. *Electronic Structure Calculations: Density Functional Methods with Application to Transition Metal Complexes*; Solomon, E. I., Lever, A. B. P., Eds.; Wiley: New York, 1999; Vol. I, pp 661−724.

increases upon oxidation as this increases the Z_{eff} of the metal ion, thus stabilizes the d-manifold, and increases the covalent interaction with the ligand. In the case of the Ni bis(dithiolene) complexes, the oxidation is more localized on the ligand, which in turn increases the Z_{eff} of the S atoms. This stabilizes the ligand orbitals relative to the metal d-manifold leading to increased mixing and, thus, a decrease in S character due to the inverted bonding description.

Bonding Description of $[Ni(S_2C_2Me_2]^{2-}$. The bonding in the square-planar, formally Ni^{II} bis(dithiolene) complex is found to be significantly different than that of the tetrahedral, tetrathiolate complex ($[Ni^{II}(S\text{-}2Ph\text{-}C_6H_5)_4]^{2-}$).[2,78] This can be seen experimentally from the strikingly different intensities of the pre-edge features in Figure 2C even taking into account the increased transition dipole integral of the dithiolene-S ($I(S^d) = 9.84$) relative to the thiolate-S ($I(S^t) = 8.05$). The bonding in the bis(dithiolene) complex is inverted (Scheme 1B) with the ligand orbitals at higher energy than the metal d-orbitals, while the tetrathiolate complex has a normal bonding description (Scheme 1A) with the metal d-orbitals at higher energy than the ligand orbitals. The LUMO reflects the nature of the uncompensated electron density of the bonding combinations, thus, the ground state bonding description. The formally Ni^{II} center of the dianionic dithiolene complex accepts electron density from the occupied σ^- orbital of the bis(dithiolene) ligand system (Figure 4B), which is higher in energy as it has an antibonding S···S interaction within and between the two enedithiolates. This removal of electron density from the σ antibonding orbital of the bis(dithiolene) ligand system results in a net bonding interaction between the dithiolenes and, consequently, in short interligand S···S distances (3.09 Å) compared to the Ni^{II} tetrathiolate complex (3.66 Å and 3.89 Å). This can be also seen by comparing the maleonitrile-dithiolate ligand ($Rb_2[S_2C_4N_2]$) to its Ni bis(dithiolene) complex ($Rb_2[Ni(S_2C_4N_2)_2]$).[79] The S···S distance in the enedithiolate salt is 3.47 Å, which is reduced to 3.13 Å in the Ni bis(dithiolene) complex. The interligand S···S distance in the complex (3.02 Å) is even shorter than the intraligand distances, indicating that a bonding interaction is also present between the dithiolene ligands.

Density functional calculations using gradient-corrected (GGA) functionals such as B88P86 or B88LYP were found to give too little ligand character for the dianionic complex. Functionals with correct asymptotic behavior, such as van Leeuwen−Baerends functional (LB94), give a more reasonable bonding description but still too little ligand character.

Bonding Description of $[Ni(S_2C_2Me_2]^{1-}$. The bonding description of the in-plane $13b_{1g}$ orbital of the monoanionic complex is as discussed for the dianionic complex. The small (6%) decrease of ligand character in this LUMO does not strongly perturb the bonding. Upon oxidation of the dianionic form, a hole is created in the out-of-plane π-system. The quantitation of the S K-edge XAS data (Figure 3 and Table 1) of this SOMO($5b_{2g}$) is in good agreement with the spin distribution obtained from EPR.[8,11,12] As discussed for the LUMO of the dianionic complex, the SOMO is also highly delocalized (S K-edge peak at 2470.0 eV in Figures 2A and 3A) with more than 50% ligand character (Table 2). The decrease of electron density in this out-of-plane antibonding orbital induces a π-type bonding interaction between the ligands and results in additional shortening of the S···S distances. From the X-ray structures, the intra- and interligand S···S distances are shortened by 0.03 Å and 0.08 Å, respectively, in the monoanionic complex relative to the dianionic complex due to the additional π-bonding and reduced ligand repulsion (*vide supra*).

The GGA density functional calculations (both spin-restricted and -unrestricted) or use of asymptotically corrected functionals in correlation with experimental data give a reasonable ground state bonding description (within 10%) of the monoanionic, paramagnetic complex. Inclusion of HF exchange does not improve the agreement between calculation and experiment.

Bonding Description of $[Ni(S_2C_2Me_2]$. The near-edge region of the S K-edge XAS spectrum (Figure 2, energy region 2473−2475 eV) of the neutral complex indicates significant changes in the electronic structure compared to those of the mono- or dianionic complexes. By removal of two electrons in going from the dianionic to the neutral complex, the ligand−ligand repulsion, as a governing factor of the electronic structure of the dithiolene complexes, is significantly reduced and therefore the ligand and the metal orbitals are energetically and geometrically closer to each other than in the anionic complexes (Ni−S bond lengths are 2.18 Å, 2.14 Å, and 2.13 Å; S−Ni−S (bite) angles are 90.1°, 90.6°, and 91.4° in $Z = 2-$, $1-$, and 0, respectively[19]).

It is interesting to compare the HOMO/LUMO gap in the neutral complex and correlate with the possibility of spin localization, which can give diradical character to the ground state wave function. In the neutral Ni bis(dithiolene) complex, the energy separation of the $6b_{1u}$ (HOMO) and the $5b_{2g}$ (LUMO) orbitals is about 1.1 eV (Figure 5). This splitting is a combined effect of (i) a direct ligand−ligand interaction of the π_3^- and π_3^+ orbitals of the bis(enedithiolate) ligand system (0.5 eV, Figure 4) due to the close proximity of the two ligands and (ii) the presence of approximately 25% Ni $3d_{xz}$ contribution in $5b_{2g}$, which can provide a superexchange pathway between the two enedithiolates. The approximately 1 eV HOMO/LUMO gap is reasonably small and can allow for limited localization. This can be seen from the presence of some spin polarization, which increases as the amount of HFX increases (Table 2, bottom and Figure 6). In contrast to the π_3 orbitals, the splitting of the in-plane orbitals (σ^- and σ^+) is much larger (3 eV, Figure 5). The large splitting of σ orbitals can be rationalized by the larger in-plane ligand−ligand repulsion due to the orientation of the S 3p lobes and the larger localization on the S atoms in comparison to the π_3 orbitals. Therefore, bonding involving these orbitals can be characterized as a strongly delocalized, covalent interaction with no spin polarization.

Spectroscopically adjusted hybrid density functionals are needed to accurately describe the experimental ground state covalency of the neutral complex. Based on the quantitation of S XAS pre-edge intensities, mixing of approximately 10% HF exchange (in between the B88P86 and the B3LYP methods) gives the most reasonable fit to the experimental data. Hybrid

(77) The ligand character of the individual orbitals is influenced by two counteracting effects: (i) upon oxidation, the electron is mainly lost from a ligand based orbital ($13b_{1g}$), which reduces the ligand−ligand repulsion and therefore stabilizes the σ^- orbital of the bis(dithiolene) ligand system (Figure 4); (ii) the S atoms in the out-of-plane π-orbitals ($5b_{2g}$) are affected less by oxidation, since they are more delocalized over the αC−αC framework than the in-plane σ-orbitals.

(78) Drager, M.; Gattow, G. *Z. Anorg. Allg. Chem.* **1972**, *391*, 203.
(79) Clemenson, P. I.; Underhill, A. E.; Kobayashi, A.; Kobayashi, U. *Polyhedron* **1990**, *9*, 2053−2059.

Scheme 2

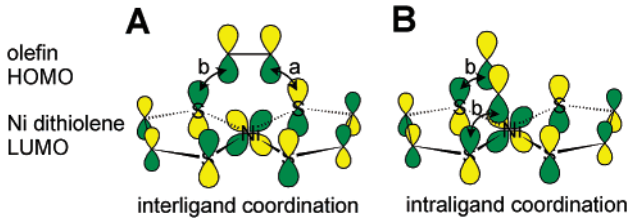

DFT calculations with more than 20% HFX give limited localization of the spin densities. The best fit of the calibrated DFT to the covalency of the paramagnetic complex based on the EPR spin distribution, B88(25HF)P86/BS5, gives only an upper limit of 0.4 electron spin density on each of the ligands, with at least 60% S character, on each dithiolene ligand with opposite sign (Table 2, bottom and Figure 6B).

Reactivity of [Ni($S_2C_2R_2$]. Recently, Wang and Stiefel have introduced a novel method for olefin separation and purification using Ni bis(dithiolene) complexes.[25] The neutral complex reacts with olefins in a nonclassical manner forming S−C bonds, rather than coordinating to the metal center in a π-complex fashion. The reaction mechanism is described as the electrophilic addition of the bis(dithiolene) complex to the olefin, which involves donating electron density from the olefin HOMO into the LUMO of the bis(dithiolene) complex. The product structure of the interligand, cis adduct was proposed on the basis of the $[Ni(S_2C_2(CF_3)_2)_2]$/norbornane reaction.[80]

The inverted bonding description and the noninnocent nature of the dithiolene ligand provide insight into this nonclassical reactivity. The frontier orbitals (LUMO and LUMO+1) of the neutral complex have a large ligand contribution, making the ligand the electron-deficient site. Atomic charges calculated by the NPA method show large polarization in the Ni−S bonds with +0.26e and −0.46e charges on the S and the Ni atoms, respectively, which also indicate the preference of the S sites for the electrophilic addition. However, the LUMO ($5b_{2g}$ with Ni $3d_{xz}$ and ligand π_3^- contributions, Figure 5) does not have the proper phases to give a net bonding with the HOMO of the ethylene molecule between the dithiolene ligands (Scheme 2A). A recent DFT study[81] showed that this orbital forbiddeness of the formation of the interligand olefin adduct can be overcome by a D_{2d} distortion of the Ni bis(dithiolene) complex. In this distorted geometry, the lobes of the olefin HOMO can overlap with the opposite sides of the LUMO lobes on the S atoms of the bis(dithiolene) complex. This addition gives a trans product, which can isomerize to the cis product. The calculated activation barrier ($\Delta G^{\ddagger}$) of the rate-limiting step (trans addition) is 113 kJ mol^{-1}, which is about 20 kJ mol^{-1} higher than the experimental value.[25] A contribution to the high activation barrier would be the D_{2d} distortion energy of the highly covalent, square-planar Ni bis(dithiolene) complex and the rotation of the C═C bond in the ethylene to form the interligand, trans adduct.

As an alternative reaction pathway, the LUMO of the neutral Ni bis(dithiolene) complex has the proper phases to overlap with the HOMO of the olefin molecule within one of the dithiolene ligands (Scheme 2B). This would favor an alternative product structure of an intraligand, cis adduct (Diels−Alder type product assuming olefin formally reacts with a dithioketone) with a lower activation barrier, since it is an orbitally allowed process and neither the Ni bis(dithiolene) complex or the olefin needs to be significantly distorted. Preliminary hybrid density functional calculations indicate that the pathways corresponding to the inter- and the intraligand coordination of the olefin molecule are comparable with a limited (12 kJ mol^{-1}) preference in the transition state energy of the latter in agreement with the above FMO analysis. The intraligand chelated product has been observed in the reaction of olefins with diphenyl-substituted dithiolene complexes.[27,82]

Finally, it should be noted that the singlet/triplet gap for the neutral dithiolene complex is relatively small (60 kJ mol^{-1} in the ground-state geometry at the B3LYP/BS6 level of theory), which is expected to decrease further by 10−20 kJ mol^{-1} due to geometric relaxation. As with the singlet ground state, the triplet state has a large S character (56% S, 7% Ni, and 37% C) nearly equally distributed between the HOMO and the LUMO of the Ni bis(dithiolene) complex, which are each singly occupied in the triplet. For the triplet, the lower energy singly occupied MO can also provide a bonding interaction with the olefin HOMO facilitating the electrophilic addition of the bis(dithiolene) complex to the olefin.

Conclusions. The EPR, ENDOR, ESEEM, and XAS results converge to a common ground state description of the monoanionic Ni bis(dithiolene) complex. In addition, gradient-corrected density functional theory (such as B88P86 with theoretically converged basis) gives a ground state electronic structure of the monoanion, which is in reasonable agreement with experiment. X-ray absorption spectroscopy allows this study to extend over the Ni bis(dithiolene) series including the dianionic and the neutral forms, which are diamagnetic. XAS pre-edge intensities at the S K-edge show that the lowest unoccupied orbitals are ligand based and have more than 50% S character in all three oxidation states. The LUMO of the dianionic complex is the in-plane, antibonding combination of Ni $3d_{xy}$ (25% est.) and S $3p_{x+y}$ (77%) orbitals of b_{1g} symmetry. The gradient-corrected density functional ground state of the dianionic form has less ligand character than observed experimentally. From experiment (Figure 2A and Table 1), the dianionic complex has an extensive charge donation from the dithiolene ligand to the Ni atom, in contrast to the $[Ni^{II}(SR)_4]^{2-}$ complex. The SOMO of the monoanionic complex is the out-of-plane, antibonding combination of Ni $3d_{xz}$ (25% est.) and S $3p_z$ (59%) orbitals of b_{2g} symmetry, while the LUMO remains essentially the same as in the dianionic complex (Figure 5). In the neutral complex, both the in-plane (b_{1g}) and the out-of-plane (b_{2g}) valence orbitals are unoccupied and are characterized by 67% and 57% S 3p, respectively, and approximately 20% Ni 3d contributions in both orbitals. Hybrid DFT calculations supported by XAS and EPR experiments indicate the presence of at most limited spin polarization (i.e., diradical character) of the dithiolene ligand. Bachler et al.[19] come to a similar conclusion for the Ni complexes of ortho-semiquinolato type ligands, where the diradical character increases in the order of S > N > O donors. On the basis of the dominant ligand character of the ground state wave functions, the bonding in all oxidation states of the Ni bis(dithiolene) complexes can be

(80) Wing, R. M.; Tustin, G. W.; Okamura, W. H. *J. Am. Chem. Soc.* **1970**, *92*, 1935−1939.
(81) Fan, Y.; Hall, M. B. *J. Am. Chem. Soc.* **2002**, *124*, 12076−12077.
(82) Schrauzer, G. N.; Rabinowitz, H. N. *J. Am. Chem. Soc.* **1968**, *90*, 4297−4302.

described as inverted (Scheme 1B), with the ligand valence orbitals at higher energy than the metal d-manifold. The destabilized ligand orbitals (due to ligand-ligand repulsion) and the good overlap with the Ni 3d orbitals allow efficient electron donation to the metal. This electron density is donated by antibonding ligand orbitals, which allows for weak bonding interaction between the two dithiolenes. This extensive electron donation also makes the dithiolene ligand electrophilic, which explains the nonclassical reactivity of dithiolene complexes with olefins.

Acknowledgment. This work was supported by NSF CHE 98-76457 (R.H.H.), NIH 28856 (R.H.H.), NIH RR-01209 (K.O.H.), and NSF CHE-9980549 (E.I.S.) grants. SSRL operations are funded by the Department of Energy, Office of Basic Energy Sciences. The SSRL Structural Molecular Biology program is supported by the National Institutes of Health, National Center for Research Resources, Biomedical Technology Program and by the Department of Energy, Office of Biological and Environmental Research. T.G. gratefully acknowledges the Deutsche Forschungsgemeinschaft for a postdoctoral fellowship. We would like to thank Dr. Serena DeBeer George and Dr. Patrick Frank for helpful discussions.

Supporting Information Available: Tables containing detailed electronic structure analysis of the free ligands (S1), basis set and population analysis calibrations for the $[Ni(S_2C_2Me_2)_2]^{2-}$ complex (S2), functional dependence of the S 3p character of the LUMO of the $[Ni(S_2C_2Me_2)_2]^{2-}$ complex in ADF, and ground-state S 3p covalencies at LB94/BSIV level. Figures containing symmetrized D_{2h} structures of $[Ni(S_2C_2Me_2]^{2-/1-/0}$ complexes used in calculations with selected internal and Cartesian coordinates (S1−S3); representative fits for paramagnetic contamination corrected S K-edge pre-edge feature and second derivative of the $(Et_4N)_2[Ni(S_2C_2Me_2]$, $(Et_4N)[Ni(S_2C_2Me_2]$, and $[Ni(S_2C_2Me_2]$ compounds (S4−S6); nickel K-edge spectra of $(Et_4N)_2[Ni(S\text{-}2Ph\text{-}C_6H_4)_4]$, $(Et_4N)_2[Ni(S_2C_2Me_2)_2]$, $(Et_4N)[Ni(S_2C_2Me_2)_2]$, and $[Ni(S_2C_2Me_2)_2]$ complexes (S7). This material is available free of charge via the Internet at http://pubs.acs.org.

JA029806K